JACS
JOURNAL OF THE AMERICAN CHEMICAL SOCIETY

Subscriber access provided by ISTANBUL TEKNIK UNIV

Article

Conformational Adaptation and Selective Adatom Capturing of Tetrapyridyl-porphyrin Molecules on a Copper (111) Surface

Willi Auwrter, Florian Klappenberger, Alexander Weber-Bargioni, Agustin Schiffrin, Thomas Strunskus, Christof Wll, Yan Pennec, Andreas Riemann, and Johannes V. Barth

J. Am. Chem. Soc., **2007**, 129 (36), 11279-11285• DOI: 10.1021/ja071572n • Publication Date (Web): 18 August 2007

Downloaded from http://pubs.acs.org on February 14, 2009

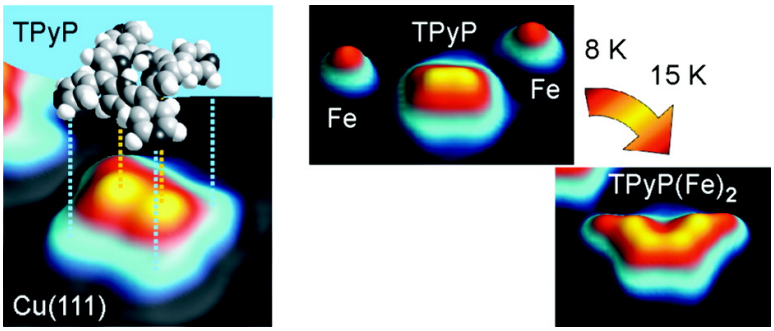

More About This Article

Additional resources and features associated with this article are available within the HTML version:

- Supporting Information
- Links to the 9 articles that cite this article, as of the time of this article download
- Access to high resolution figures
- Links to articles and content related to this article
- Copyright permission to reproduce figures and/or text from this article

View the Full Text HTML

ACS Publications
High quality. High impact.

Journal of the American Chemical Society is published by the American Chemical Society. 1155 Sixteenth Street N.W., Washington, DC 20036

J|A|C|S
ARTICLES
Published on Web 08/18/2007

Conformational Adaptation and Selective Adatom Capturing of Tetrapyridyl-porphyrin Molecules on a Copper (111) Surface

Willi Auwärter,*[,†,‡,⊥] Florian Klappenberger,[‡,⊥] Alexander Weber-Bargioni,[†] Agustin Schiffrin,[†] Thomas Strunskus,[§] Christof Wöll,[§] Yan Pennec,[†] Andreas Riemann,[†,||] and Johannes V. Barth[†,⊥]

Contribution from the Departments of Chemistry and Physics and Astronomy, University of British Columbia, Vancouver, BC V6T1Z4, Canada, Ecole Polytechnique Fédérale de Lausanne, Institut de Physique des Nanostructures, CH-1015 Lausanne, Switzerland, Lehrstuhl für Physikalische Chemie I, Ruhr-Universität Bochum, D-44780 Bochum, Germany, and Physik Department E20, Technische Universität München, D-85748 Garching, Germany

Received March 6, 2007; E-mail: wilhelm.auwaerter@ph.tum.de

Abstract: We present a combined low-temperature scanning tunneling microscopy and near-edge X-ray adsorption fine structure study on the interaction of tetrapyridyl-porphyrin (TPyP) molecules with a Cu-(111) surface. A novel approach using data from complementary experimental techniques and charge density calculations allows us to determine the adsorption geometry of TPyP on Cu(111). The molecules are centered on "bridge" sites of the substrate lattice and exhibit a strong deformation involving a saddle-shaped macrocycle distortion as well as considerable rotation and tilting of the meso-substituents. We propose a bonding mechanism based on the pyridyl−surface interaction, which mediates the molecular deformation upon adsorption. Accordingly, a functionalization by pyridyl groups opens up pathways to control the anchoring of large organic molecules on metal surfaces and tune their conformational state. Furthermore, we demonstrate that the affinity of the terminal groups for metal centers permits the selective capture of individual iron atoms at low temperature.

1. Introduction

The control of large functional molecules at metallic substrates is of great interest and plays a central role in various fields in science and technology, ranging from heterogeneous catalysis[1] to molecular electronics,[2] optoelectronics based on organic thin films,[3] or single-molecule contacts.[4,5] The surface chemical bonding steers the mobility of the adsorbed molecular building blocks,[6] which is decisive for a controlled self-assembly of functional architectures on the nanoscale.[7] Furthermore, the interaction of complex molecules exhibiting internal degrees of freedom with the substrate frequently induces modifications of the molecular configuration, be it a conformational adaptation or a change in the chemical composition or electronic structure.[8] These effects are reflected in a varied chemical reactivity, induced charge transfer, or altered magnetic properties.[9] Thus it is of fundamental interest to determine the adsorption geometry, i.e., the internal conformation, as well as the adsorption site of the molecule on the substrate atomic lattice. This set of information makes it possible to categorize adsorbate−substrate interactions and yields a basis for a theoretical discussion of important issues as bonding mechanisms, bond energies, electronic level alignment, or functional properties based on conformational or supramolecular design. In addition, it is important to probe the lateral reactivity of complex molecular species anchored at surfaces with peripheral functional groups in view of their aptitude for the formation of (metallo)-supramolecular compounds and networks.

Because of its excellent real space imaging capabilities scanning tunneling microscopy (STM) is ideally suited to observe, characterize, and manipulate individual molecules on conducting substrates. Notably, the conformation,[10−12] mobil-

[†] University of British Columbia.
[‡] Ecole Polytechnique Fédérale de Lausanne.
[§] Ruhr Universität Bochum.
[⊥] Technische Universität München.
[||] Current address: Department of Physics and Astronomy, Western Washington University, Bellingham, WA 98225−9164.

(1) (a) Castonguay, M.; Roy, J. R.; Rochefort, A.; McBreen, P. H. *J. Am. Chem. Soc.* **2000**, *122*, 518−524. (b) Barlow, S. M.; Raval, R. *Surf. Sci. Rep.* **2003**, *50*, 201−341.
(2) Joachim, C.; Gimzewski, J. K.; Aviram, A. *Nature* **2000**, *408*, 541−548.
(3) (a) Forrest, S. R. *Chem. Rev.* **1997**, *97*, 1793−1896. (b) Ishii, H.; Sugiyama, K.; Ito, E.; Seki, K. *Adv. Mater.* **1999**, *11*, 605−625.
(4) Nazin, G. V.; Qiu, X. H.; Ho, W. *Science* **2003**, *302*, 77−81.
(5) (a) Moresco, F.; Gross, L.; Alemani, M.; Rieder, K.-H.; Tang, H.; Gourdon, A.; Joachim, C. *Phys. Rev. Lett.* **2003**, *91*, 036601−036604. (b) Grill, L.; Rieder, K.-H.; Moresco, F.; Stojkovic, S.; Gourdon, A.; Joachim, C. *Nano Lett.* **2005**, *5*, 859−863.
(6) Schunack, M.; Linderoth, T. R.; Rosei, F.; Laegsgaard, E.; Stensgaard, I.; Besenbacher, F. *Phys. Rev. Lett.* **2002**, *88*, 156102.
(7) (a) Barth, J. V.; Costantini, G.; Kern, K. *Nature* **2005**, *437*, 671−679. (b) Barth, J. V. *Annu. Rev. Phys. Chem.* **2007**, *58*, 375−407.
(8) (a) Rosei, F.; Schunack, M.; Naitoh, Y.; Jiang, P.; Gourdon, A.; Laegsgaard, E.; Stensgaard, I.; Joachim, C.; Besenbacher, F. *Prog. Surf. Sci.* **2003**, *71*, 95−146. (b) Hauschild, A.; Karki, K.; Cowie, B. C. C.; Rohlfing, M.; Tautz, F. S.; Sokolowski, M. *Phys. Rev. Lett.* **2005**, *94*, 036106.
(9) Iancu, V.; Deshpande, A.; Hla, S.-W. *Nano Lett.* **2006**, *6*, 820−823.
(10) Jung, T. A.; Schlittler, R. R.; Gimzewski, J. K. *Nature* **1997**, *386*, 696.

ity,[13] and self-assembly[14,15] of porphyrin species on metal surfaces attracted considerable interest in recent years. This class of molecules exhibits an intriguing variety of functional properties, which are exploited in both biological and artificial systems.[16] Accordingly, these versatile molecules are promising building blocks to assemble functional nanostructures on surfaces, specifically opening up new opportunities to build sensors and nanoscale optical and magnetic materials.[17] In the context of this article it is relevant to mention two features connected to the functionality of porphyrins. The rotational degrees of freedom of the chosen meso-substituents and the flexibility of the porphyrin macrocycle allow for a conformational adaptation of the molecule to its local environment. Relative to the molecular core, the conformation of the leg is determined by two angles (θ and ϕ), which are indicated in Scheme 1. The angle θ describes the rotation of a pyridyl group around the C−C bond connecting it to the porphyrin core, while ϕ indicates a bending of this C−C bond out of the macrocycle plane.[11] To some extent, the dihedral angle θ and the nonplanar deformation (ρ) of the macrocycle are interconnected through steric repulsion between hydrogen atoms of the ring and the hydrogens of the porphyrin macrocycle. Accordingly, many reports on macrocycle distortions as well as varying dihedral angles are available for solid-state phases.[18,19] On surfaces, however, the vast majority of studies focus solely on the orientation[10,11,15] and considerate manipulation[20,21] of the meso-substituents. Only some recent reports speculate on nonplanar adsorption geometries;[9,12,22] however, by pure STM imaging the question of intramolecular structure cannot be quantitatively addressed.

Meso-substituted porphyrins with a wide variety of endgroups can be synthesized. This provides a series of building blocks for metal−organic networks in solid-state chemistry.[23] Specifically tetraaryl-porphyrins functionalized by pyridyl substituents interact via the terminal nitrogen lone pair with a wide variety of reactive metal centers (Cu,[24,25] Fe,[26] Pd,[27] Pb[28]) to form ordered structures. By contrast, on surfaces, the pyridyl-mediated interaction of porphyrins with the substrate or coadsorbed atoms was not explored to date. Nevertheless, the considerate choice of substituents with specific chemical or electrostatic characteristics allows one to tune the adsorbate−adsorbate interaction[29] and thus to assemble not only supramolecular aggregates with controlled size and shape[30] but also nanoporous host networks.[31]

Here, we focus on the detailed understanding and control of adsorbate−substrate interactions. By employing a nitrogen termination, it is possible to anchor tetrapyridyl-porphyrin (TPyP) on the smooth Cu(111) surface and to restrict molecular

Scheme 1. Model of an Isolated Tetrapyridyl-porphyrin (TPyP) Molecule in Its Gas-Phase Conformation[a]

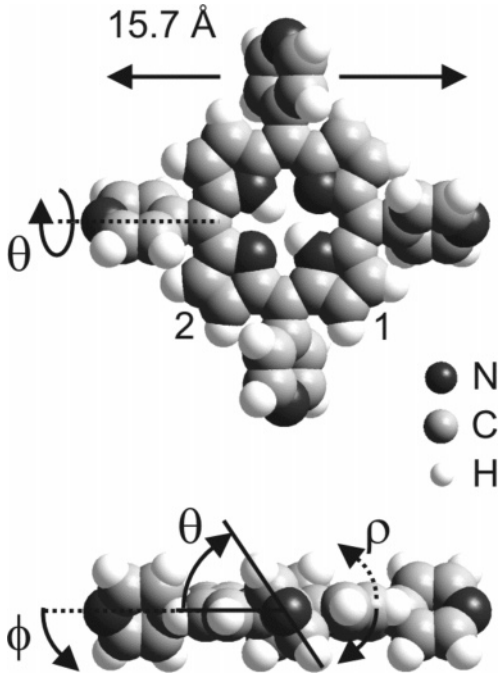

[a] The top view (upper panel) highlights the central porphyrin core consisting of inequivalent pyrrole rings (labeled 1 and 2) and the four terminal pyridyl groups, the legs. In the side view (lower panel) we indicate the two angles (θ and ϕ), which determine the conformation of the legs relative to the porphyrin macrocycle (the $\theta = 90°$ and $\phi = 0°$ situation means that the pyridyl groups are oriented perpendicular to the porphyrin plane, while the C−C bonds connecting the legs to the core are aligned parallel to the surface). A possible nonplanar deformation of the latter is described by the angle ρ ($\rho = 0°$ corresponds to a planar macrocycle).

(11) Moresco, F.; Meyer, G.; Rieder, K.-H.; Ping, J.; Tang, H.; Joachim, C. *Surf. Sci.* **2002**, *499*, 94−102.
(12) Yokoyama, T.; Yokoyama, S.; Kamikado, T.; Mashiko, S. *J. Chem. Phys.* **2001**, *115*, 3814.
(13) (a) Ogaki, K.; Batina, N.; Kunitake, M.; Itaya, K. *J. Phys. Chem.* **1995**, *100*, 7185−7190. (b) Kunitake, M.; Akiba, U.; Batina, N.; Itaya, K. *Langmuir* **1997**, *13*, 1607−1615. (c) Shimada, T.; Hashimoto, R.; Koide, J.; Kamimuta, Y.; Koma, A. *Surf. Sci.* **2000**, *470*, L52−L56. (d) He, Y.; Ye, T.; Borguet, E. *J. Am. Chem. Soc.* **2002**, *124*, 11964−11970. (e) Suto, K.; Yoshimoto, S.; Itaya, K. *Langmuir* **2006**, *22*, 10766−10776. (f) Suzuki, H.; Berner, S.; Brunner, M.; Yanagi, H.; Schlettwein, D.; Jung, T. A.; Güntherodt, H.-J. *Thin Solid Films* **2001**, *393*, 325−328.
(14) (a) Scudiero, L.; Barlow, D. E.; Hipps, K. W. *J. Phys. Chem. B* **2000**, *104*, 11899−11905. (b) Scudiero, L.; Hipps, K. W.; Barlow, D. E. *J. Phys. Chem. B* **2003**, *107*, 2903−2909.
(15) Auwärter, W.; Weber-Bargioni, A.; Riemann, A.; Schiffrin, A.; Groening, O.; Fasel, R.; Barth, J. V. *J. Chem. Phys.* **2006**, *124*, 194708.
(16) (a) *The Porphyrins*; Dolphin, D., Ed.; Academic: New York, 1978. (b) Milgrom, L. R. *The Colours of Life: An Introduction to the Chemistry of Porphyrins and Related Compounds*; Oxford University Press: Oxford, 1997.
(17) (a) *The Porphyrin Handbook Vol. 6, Applications: Past, Present and Future*; Kadish, K. M., Schmith, K. M., Guilard, R., Eds.; Academic Press: San Diego, 2000; Vol. 6. (b) Elemans, J. A. A. W.; Hameren, R. v.; Nolte, R. J. M.; Rowan, A. E. *Adv. Mater.* **2006**, *18*, 1251−1266.
(18) (a) Pan, L.; Kelly, S.; Huang, X.; Li, J. *Chem. Commun.* **2002**, 2334−2335. (b) Marques, H. M.; Brown, K. L. *Coord. Chem. Rev.* **2002**, *225*, 123−158. (c) Fleischer, E. B.; Miller, C. K.; Webb, L. E. *J. Am. Chem. Soc.* **1964**, *86*, 2342−2347. (d) Silvers, S. J.; Tulinsky, A. *J. Am. Chem. Soc.* **1967**, *89*, 3331−3337.
(19) Shelnutt, J. A.; Song, X.-Z.; Ma, J. G.; Jia, S.-L.; Jentzen, W.; Medforth, C. J. *Chem. Soc. Rev.* **1998**, *27*, 31−41.
(20) Moresco, F.; Meyer, G.; Rieder, K.-H.; Tang, H.; Gourdon, A.; Joachim, C. *Phys. Rev. Lett.* **2001**, *86*, 672−675.
(21) Loppacher, C.; Guggisberg, M.; Pfeiffer, O.; Meyer, E.; Bammerlin, M.; Luthi, R.; Schlittler, R.; Gimzewski, J. K.; Tang, H.; Joachim, C. *Phys. Rev. Lett.* **2003**, *90*, 066107.
(22) (a) Qiu, X. H.; Nazin, G. V.; Ho, W. *Phys. Rev. Lett.* **2004**, *93*, 196806. (b) Auwärter, W.; Weber-Bargioni, A.; Brink, S.; Riemann, A.; Schiffrin, A.; Ruben, M.; Barth, J. V. *Chem. Phys. Chem.* **2007**, *8*, 250−254.
(23) (a) Fujita, M. *Chem. Soc. Rev.* **1998**, *27*, 417−425. (b) Kosal, M. E.; Suslick, K. S. *J. Solid State Chem.* **2000**, *152*, 87.
(24) Abrahams, B. F.; Hoskins, B. F.; Michail, D. M.; Robson, R. *Nature* **1994**, *369*, 727−729.
(25) Hagrman, D.; Hagrman, P. J.; Zubieta, J. *Angew. Chem., Int. Ed.* **1999**, *38*, 3165−3168.
(26) Pan, L.; Kelly, S.; Huang, X.; Li, J. *Chem. Commun.* **2002**, 2334−2335.
(27) Drain, C. M.; Nifiatis, F.; Vasenko, A.; Batteas, J. D. *Angew. Chem., Int. Ed.* **1998**, *37*, 2344−2347.
(28) Sharma, C. V. K.; Broker, G. A.; Huddleston, J. G.; Baldwin, J. W.; Metzger, R. M.; Rogers, R. D. *J. Am. Chem. Soc.* **1999**, *121*, 1137−1144.
(29) Lei, S. B.; Wang, C.; Yin, S. X.; Wang, H. N.; Xi, F.; Liu, H. W.; Xu, B.; Wan, L. J.; Bai, C. L. *J. Phys. Chem. B* **2001**, *105*, 10838−10841.
(30) Yokoyama, T.; Yokoyama, S.; Kamikado, T.; Okuno, Y.; Mashiko, S. *Nature* **2001**, *413*, 619−621.
(31) (a) Spillmann, H.; Kiebele, A.; Jung, T. A.; Bonifazi, D.; Cheng, F.; Diederich, F. *Adv. Mater.* **2006**, *18*, 275−279. (b) Kiebele, A.; Bonifazi, D.; Cheng, F.; Stöhr, M.; Diederich, F.; Jung, T.; Spillmann, H. *Chem. Phys. Chem.* **2006**, *7*, 1462−1470.

diffusion even at room temperature. The underlying binding mechanism locks the molecule into specific positions on the substrate lattice and induces a considerable deformation of TPyP. A saddle-shape conformational adaptation is determined by a combination of STM and near-edge X-ray adsorption fine structure (NEXAFS) measurements and further specified with image simulations based on semiempirical methods. Additionally, we directly investigate the potential of the conformationally adapted species for lateral metal−organic linkages by monitoring the affinity of metal centers to the pyridyl groups, which can be selectively decorated by coadsorbed Fe adatoms at low temperatures.

2. Experimental Section

All STM experiments were performed in a custom-designed ultrahigh vacuum (UHV) apparatus comprising a commercial low-temperature STM[32] based on a design described elsewhere.[33] The system base pressure is below 2×10^{-10} mbar.

The Cu(111) single-crystal surface was cleaned by repeated cycles of Ar^+ sputtering (800 eV) followed by annealing to 780 K. Subsequently, TPyP (97+% purity, Frontier Scientific) was deposited by organic molecular beam epitaxy (OMBE) from a quartz crucible held at 525 K. Typical evaporation rates are roughly 0.03 monolayer/min (one monolayer corresponds to a densely packed molecular film). TPyP was thoroughly degassed prior to any experiments resulting in a background pressure in the 10^{-10} mbar range during deposition. After dosing TPyP at room temperature, the sample was cooled down and transferred into the STM, where constant current images were recorded at about 11 K using electrochemically etched tungsten tips. In the figure captions *V* refers to the bias voltage applied to the sample.

High-purity carbon monoxide (CO) gas was dosed in situ at sample temperatures not exceeding 18 K. Fe atoms were evaporated from a homemade water-cooled cell by resistively heating a W filament surrounded by an Fe wire of high purity (99.998%). Our experimental setup allows direct access of the atomic beam to the sample placed in the STM.

The NEXAFS data were taken at the HE-SGM beamline at BESSY II in Berlin at TPyP coverages close to a full monolayer. For the measurements at the N K edge the partial electron yield mode (retarding voltage 270 V) was used. The energy resolution was approximately 0.5 eV. All spectra have been referenced against a characteristic peak (399 eV) in simultaneously recorded spectra of a contaminated Au grid. For each incidence angle an average of four spectra is presented. To concentrate on the information related to the TPyP adsorbate layer, we processed the raw data by subtracting the signal of the bare crystal, then corrected for the transmission through the beamline, and finally normalized the edge jump to one at 430 eV. Comparing X-ray photoelectron spectra as well as NEXAFS data taken before and after extended irradiation of the sample, we conclude that under the given experimental conditions no effects of beam damage occurred.

As a basis to corroborate and analyze the experimental structural data, we applied basic molecular mechanics calculations to optimize the geometry of TPyP moieties. Specifically, the MM+ force field of the Hyperchem 7.5 molecular modeling package[34] was used to calculate and minimize the total energy of the system.

The STM image simulations are based on semiempirical extended Hückel calculations,[34] which are an established tool for the interpretation of STM data.[35] A constant electron density contour is obtained by integrating over the relevant molecular orbitals, which mimics a constant current STM image.[36] Despite ignoring the substrate, this procedure proved to reliably reproduce the appearance of adsorbed molecules,[37] including TPyP on the Ag(111) surface.[15] These simulations tacitly assume that the substrate mainly modifies the alignment of frontier orbital energies and broadens discrete molecular levels into resonances, which assumptions are supported by recent theoretical work.[38]

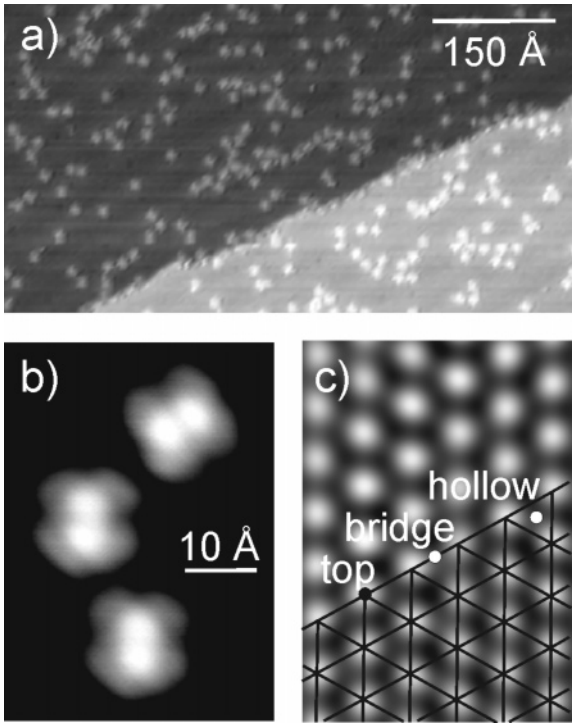

Figure 1. TPyP adsorption on Cu(111) at room temperature: (a) large-scale STM topograph depicting a random distribution of TPyP molecules on the Cu terraces ($V = -1.1$ V, $I = 0.17$ nA); (b) high-resolution STM image revealing intramolecular features ($V = -0.5$ V, $I = 0.35$ nA); (c) the Cu(111) atomic lattice. High-symmetry adsorption sites are marked ($V = 27$ mV, $I = 0.65$ nA).

3. Results and Discussion

3.1. Molecular Appearance and Adsorption Site. Figure 1a shows a large-scale STM image of two Cu(111) terraces after submonolayer deposition of TPyP at 300 K. Isolated bright spots, which are randomly distributed on the surface, are clearly discernible. High-resolution data as displayed in Figure 1b reveal that each of these protrusions corresponds to a single TPyP molecule, whereby only one species is observed.[39] The findings that TPyP neither self-assembles into highly ordered agglomerates nor considerably decorates the step edges signals appreciable interaction between the molecule and the Cu(111) surface. This restricts the mobility of TPyP on Cu(111), in marked contrast to the adsorption of the very same molecule on the less reactive Ag(111) surface, where extended islands are formed even well below room temperature.[15] STM images with intramolecular resolution (cf., Figure 1b) permit us to define a symmetry axis running through the two bright protrusions close to the center of the molecule. These axes of individual

(32) Createc GMBH, D-74391 Erligheim, Germany.
(33) Meyer, G. *Rev. Sci. Instrum.* **1996**, *67*, 2960−2965.
(34) *HYPERCHEM*; Hypercube Inc.: Gainesville, FL.
(35) Sautet, P.; Joachim, C. *Chem. Phys. Lett.* **1991**, *185*, 23−30.
(36) Gröning, O.; Fasel, R. *STM generator software*; EMPA Materials Science and Technology: Thun, Switzerland, 2004.
(37) (a) Fasel, R.; Parschau, M.; Ernst, K. H. *Nature* **2006**, *439*, 449−452. (b) Fasel, R.; Parschau, M.; Ernst, K. H. *Angew. Chem., Int. Ed.* **2003**, *42*, 5178−5181.
(38) (a) Hesper, R.; Tjeng, L. H.; Sawatzky, G. A. *Europhys. Lett.* **1997**, *40*, 177−182. (b) Neaton, J. B.; Hybertsen, M. S.; Louie, S. G. *Phys. Rev. Lett.* **2006**, *97*, 216405.
(39) Molecules embedded in between neighbors exhibit the same appearance as isolated molecules in the STM data.

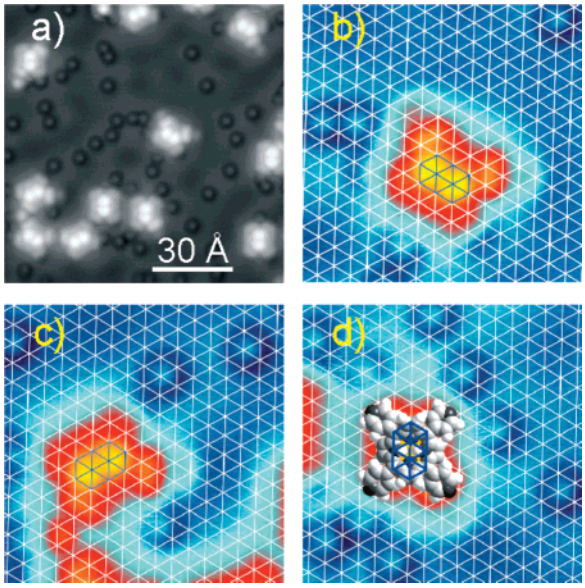

Figure 2. Adsorption site determination of TPyP on Cu(111) by using CO molecules as markers. The top left panel demonstrates the simultaneous imaging of CO and TPyP. The three color-coded plots show that TPyP is centered on the bridge site of the underlying Cu(111) lattice (compare Figure 1c, lattice constant 2.55 Å), irrespective of the azimuthal orientation ($V =$ 250 mV, $I = 0.2$ nA). The model in (d) illustrates the position of the center of the molecule.

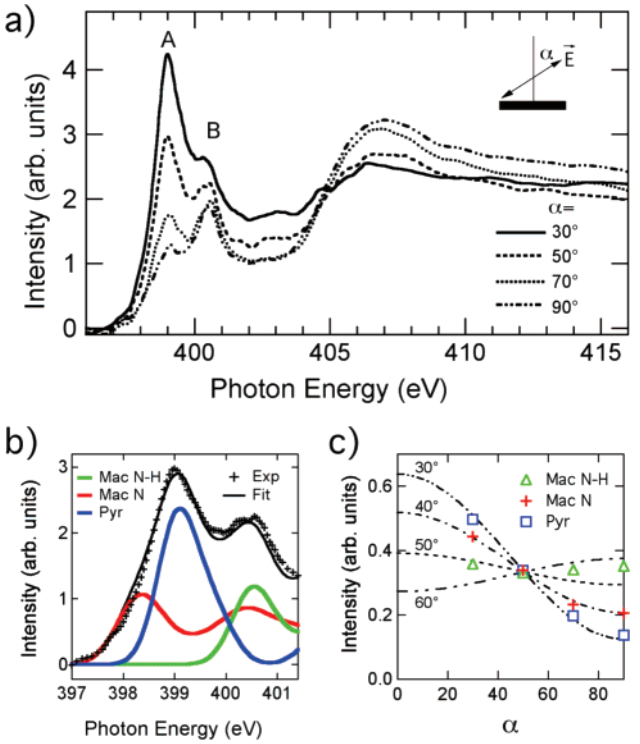

Figure 3. Analysis of the NEXAFS data indicates a strong and asymmetric distortion of the macrocycle and an endgroup inclination angle of 30°. (a) Nitrogen K edge spectra (NEXAFS) of one monolayer TPyP on Cu(111) exhibiting strong dichroism. The definition of the photon incidence angle α is shown. (b) An example showing the decomposition of the leading edge of the spectra with $\alpha = 50°$ into the three parts originating from the three chemically different nitrogen atoms. (c) The angle dependence of the intensities of the three spectral parts with theoretical curves for different angles (30−60°) between a molecular π^* resonance and the substrate.

TPyP molecules align along the close-packed ⟨110⟩ high-symmetry directions of the Cu(111) substrate, as inferred by imaging the atomic lattice (see Figure 1c). Thus, three possible azimuthal orientations of TPyP on Cu(111) exist, which are all observed in the experimental data. Besides the two prominent maxima, one can identify four broad lobes. From the molecular dimensions (side length ∼12 Å), we assign each lobe to one of the pyridyl legs. The overall appearance of TPyP on Cu(111) thus strongly deviates from the one observed on Ag(111), which is imaged with a rectangular envelope and a depression in the center.[15] As in the latter case the molecule proved to be very close to its natural gas-phase configuration (compare Scheme 1), the topographic appearance on Cu(111) points to a strong distortion of TPyP and thus to an adsorption-induced modification of the molecular conformation. An alternative explanation for the topographic images based solely on electronic effects due to molecule−substrate interactions can be ruled out (vide infra).

Before addressing this issue in more detail, we discuss the adsorption site of TPyP on Cu(111). The observation of individual molecules azimuthally oriented along substrate high-symmetry directions indicates that TPyP is located at specific sites of the underlying Cu(111) lattice. Prior to any further discussion on the molecular conformation, we verify this assumption and determine the adsorption site.

Due to incompatible imaging parameters, it is not possible to simultaneously resolve the substrate lattice and the adsorbed TPyP molecule. As an alternative solution, we applied coadsorbed CO molecules as markers to determine the adsorption site of TPyP. Related approaches were successfully used to obtain the adsorption site of adatoms and molecules.[40] It is well-known that at low coverage CO molecules stand upright and occupy exclusively "on top" positions on the Cu(111) lattice.[41] Additionally, TPyP and CO molecules can easily be imaged simultaneously by STM. This is illustrated in Figure 2a: after a minute of exposure to CO, dosed in situ at a sample temperature of 18 K, dim sombrero-shaped protrusions representing single CO molecules are visible in between the TPyP molecules. By matching a hexagonal grid representing the Cu(111) lattice (compare Figure 1c) with the positions of the CO molecules, one can conclude that the TPyP molecules are centered on "bridge" sites, irrespective of which of the three azimuthal orientations they follow (cf., Figure 2). The dissimilar appearance of the legs is tentatively explained by partial CO attachment and height modulations due to surface state scattering, which results in rings of increased apparent height surrounding CO molecules (cf., Figure 2).

3.2. Molecular Conformation. We succeeded to determine the molecular conformation of TPyP on Cu(111) by the use of a novel procedure based on two steps. First we apply NEXAFS measurements, which yield information on the dihedral angles between the molecular π systems and the surface plane. Subsequently, we refine the NEXAFS results by comparing simulated STM images with the experimental high-resolution data. The nitrogen K edge of a monolayer of TPyP on Cu(111) (Figure 3a) is dominated by two peaks, A and B (399.4 and

(40) (a) Meyer, G.; Zöphel, S.; Rieder, K. H. *Phys. Rev. Lett.* **1996**, *77*, 2113−2116. (b) Repp, J.; Meyer, G.; Stojkovic, S. M.; Gourdon, A.; Joachim, C. *Phys. Rev. Lett.* **2005**, *94*, 026803. (c) Böhringer, M.; Schneider, W.-D.; Glöckler, K.; Umbach, E.; Berndt, R. *Surf. Sci.* **1998**, *419*, L95−L99. (d) Ohara, M.; Kim, Y.; Kawai, M. *Jpn. J. Appl. Phys.* **2005**, *44*, 5390−5392.

(41) (a) Ishi, S.; Ohno, Y.; Viswanathan, B. *Surf. Sci.* **1985**, *161*, 349−372. (b) Raval, R.; Parker, S. F.; Pemble, M. E.; Hollins, P.; Pritchard, J.; Chesters, M. A. *Surf. Sci.* **1988**, *203*, 353−377.

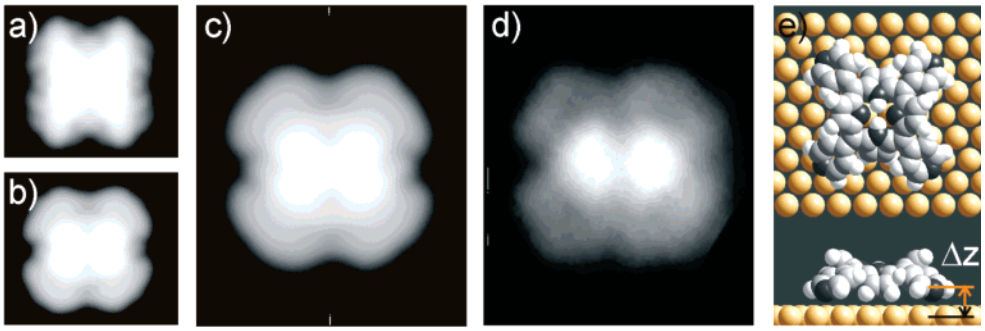

Figure 4. Comparison of simulated STM images based on molecular geometries compatible with the NEXAFS results (a−c) with an experimental STM topograph (d) ($V = -0.5$ V, $I = 0.15$ nA, width 19 Å). (e) Adsorption geometry of TPyP on Cu(111). Top view (top) and side view (bottom) clearly reveal the molecular distortion, i.e., a saddle-shaped macrocycle deformation as well as flexure of the pyridyl moieties, upon adsorption.

400.9 eV), in the π^* region, and a broad σ^* structure. The pronounced dichroism indicates well-ordered adsorption with a distinct conformation. In comparison with the spectra of a multilayer of the same molecule (not shown) the peaks are broadened and exhibit a different dependence on the incidence angle α: In the multilayer the intensity of peak A remains unchanged and the intensity of peak B is strongly reduced for $\alpha = 90°$. Contrary, adsorbed on the surface peak A decreases and peak B becomes more pronounced when increasing α. Thus, the adsorbed conformation must deviate strongly from the gas-phase conformation. For a quantitative analysis we need to decompose the spectra in parts stemming from the different molecular subgroups. To this end we focus on the π^* range, as the broad σ^* features prohibit a reliable analysis. TPyP features three chemically different nitrogen atoms, each being responsible for a part of the spectra.

The leading edge of the TPyP spectra (Figure 3b) was fitted with two macrocycle-type parts for the macrocycle nitrogen atoms without (red line, Mac N, labeled 2 in Scheme 1) and with (green line, Mac N−H, labeled 2 in Scheme 1) a hydrogen atom and one pyridylic part (blue line). To this end, we mimicked the shape of each part stemming from a macrocycle nitrogen atom by fitting typical metal−porphyrin data.[42,43] The part originating from a nitrogen atom in the substituents was fitted to data for pyridine.[43,44] In both cases the broadening of the peaks due to the interaction with the Cu substrate was taken into account. Then, we fixed the shape of the parts, i.e., the relative energy positions and the relative intensities of the peaks making up one part, and adjusted the absolute energy positions to agree with our data. Thus, the leading edge was fitted with only three fit parameters, namely, the intensities of the three parts. The corresponding angle dependences can be seen in Figure 3c, where we plotted the normalized intensities of the three parts to theoretical curves for π^* resonances with 3-fold symmetry.[45] It follows that the pyridyl endgroups have an angle of 30° (inset, solid line) with the substrate. For the normals on the pyrrole groups 1 and 2 approximate values of $\rho_1 = 50°$ and $\rho_2 = 40°$ are indicated.[46]

These findings clearly demonstrate a strong distortion of TPyPs macrocycle upon adsorption and hint to two different deformation angles ρ for the two different pyrrole groups. However, it is important to realize that the three values determined by NEXAFS do not allow for an unequivocal determination of all three important intramolecular angles and, thus, the geometry of the molecule. The conformation of the pyridyl legs relative to the porphyrin macrocycle[47] is defined by the two angles θ and ϕ introduced before (cf., Scheme 1), whereas NEXAFS only yields the inclination between the pyridyl groups and the surface. Thus, there are many possible combinations of θ and ϕ angles, which are consistent with the single value given by NEXAFS.

To resolve the molecular conformation despite this limitation, we simulated STM images for a set of geometries (cf., Figure 4a−c), which are compatible with the NEXAFS data, and compared them to a typical experimental image (see Figure 4d). This scan was recorded at a low negative sample bias voltage, thus representing occupied electronic states. Accordingly, all the calculated STM images presented below are based on the density of states of the highest occupied molecular orbitals (HOMO and HOMO-1).[48] Figure 4a shows a simulated STM image of TPyP. It represents a geometry, which was obtained by reducing the dihedral angle θ to 30° while keeping the C−C bond parallel to the surface ($\phi = 0$). This pyridyl conformation goes hand in hand with a saddle-shaped distortion of the molecular core:[19] the pyrrole rings are tilted by an angle ρ of about 40°. The simulated image is dominated by two longish protrusions, which extend to the far ends of the molecule. Obviously, this contour bears no close resemblance to the experimental STM image presented in Figure 4d. The poor agreement between calculated and measured STM topographs permits us to discard this molecular conformation and compels us to consider a bending of the C−C bond out of the macrocycle plane.

Accordingly, we freeze the pyridyl conformation by setting the angles to $\theta = 10°$ and $\phi = 20°$ and apply an average macrocycle distortion ρ of 35°. The resulting charge density image (Figure 2b) mimics the experimental data well. Both the

(42) Jong, M. P. d.; Friedlein, R.; Sorensen, S. L.; Öhrwall, G.; Osikowicz, W.; Tengsted, C.; Jönsson, S. K. M.; Fahlman, M.; Salaneck, W. R. *Phys. Rev. B* **2005**, *72*, 035448.
(43) Cudia, C. C.; Vilmercati, P.; Larciprete, R.; Cepek, C.; Zampiere, G.; Sangaletti, L.; Pagliara, S.; Verdini, A.; Cossaro, A.; Floreano, L.; Morgante, A.; Petaccia, L.; Lizzit, S.; Battocchio, C.; Polzonietti, G.; Goldoni, A. *Surf. Sci.* **2006**, *600*, 4013−4017.
(44) Kolczewski, C.; Püttner, R.; Plashkevych, O.; Ågren, H.; Staemmler, V.; Martins, M.; Snell, G.; Schlachter, A. S.; Sant'Anna, M.; Kaindl, G.; Pettersson, L. G. M. *J. Chem. Phys.* **2001**, *115*, 6426−6437.
(45) Stöhr, J. *NEXAFS Spectroscopy and the Structure of Molecules Bonded to Surfaces*; Springer: Heidelberg, Germany, 1991.

(46) The error bar for all the angles determined by NEXAFS amounts to ±10°.
(47) Here, the macrocycle plane is defined by the four meso-carbon atoms. This description holds also in the case of a saddle-shaped distortion of the porphyrin core.
(48) Including lower lying occupied molecular orbitals did not significantly improve the simulated appearance.

two central maxima and the appearance of the legs are reproduced. Furthermore, one can distinguish two different types of indentations along and perpendicular to the molecular axis, respectively.

Finally, Figure 4c shows the calculated charge density for a slightly varied geometry ($\theta = 0°$, $\phi = 30°$, $\rho_1 = 45°$, $\rho_2 = 35°$). Considering the simplicity of the applied procedure, the agreement between experiment and calculations is striking. Not only is the molecular outline nicely reproduced but also the positions of the two central maxima improved in comparison to Figure 4b. In addition, a close inspection of the macrocycle distortion ρ of this optimized geometry[49] reveals two differing angles $\rho_1 = 45°$ and $\rho_2 = 35°$ for the pyrrole rings with (1) and without hydrogen (2), respectively. The disparity of the deformation angles of these rings agrees with the NEXAFS data. Within the error bars, these values match the two angles $\rho_1 = 50°$ and $\rho_2 = 40°$ determined by NEXAFS.

In summary, a molecular conformation characterized by pyridyl rings, which are heavily rotated around the C−C bond ($\theta \leq 10°$) and additionally bent toward the substrate ($20° \leq \phi \leq 30°$) inducing a saddle-shaped macrocycle distortion ($35° \leq \rho \leq 50°$), describes the experimental results best.

Already knowing the adsorption site, we thus can establish a complete model for the adsorption geometry of TPyP on Cu(111), which is depicted in Figure 4e. To our knowledge, this is one of very few examples where STM and complementary techniques permitted the determination of the full adsorption geometry of a large functional molecule, i.e., conformation and adsorption site. Furthermore, total energy calculations in the MM+ framework indicate that the pyridyl nitrogens are separated by about 2.5 Å (Δz) from the surface plane defined by the atomic centers. The distance of the pyrrole nitrogens from the substrate is considerably larger.

Now we briefly address the possible reasons for the strong deformation of TPyP upon adsorption on Cu(111). An inspection of Figure 4e reveals that there are two groups of atoms closest to the surface: the pyridyl nitrogens and the outer pyrrolic hydrogens. Judging from the high affinity of the nitrogen to metals discussed in the introduction, the attractive N−Cu interaction is most likely the trigger for the deformation. A close distance between pyridylic N and the Cu surface atoms can only be achieved for small dihedral angles θ and a tilt of the pyridyl leg toward the substrate. As a result, the marked distortion of the porphyrin macrocycle is induced by steric constraints as a consequence of the bending of the legs.

According to this scheme, the energy necessary to distort the macrocycle should be overcompensated by the energy gain from the pyridyl−Cu interaction. Indeed the following values corroborate this interpretation. The calculated difference in total energy between a planar and a saddle-shaped tetraphenylporphyrin (TPP) molecule amounts to 26.7 kcal/mol.[12] This value is relevant for our discussion, as it is based on a nonplanar molecular conformation very similar to our case involving both a saddle-shaped deformation of the macrocycle and a tilting and twisting of the meso-substituents. Furthermore, the number is in reasonable agreement with the energy needed to induce a saddle-shaped macrocycle deformation (~2 kcal/mol[50]) *plus* the energy required for the rotation of all four meso-substituents (~40 kcal/mol[21]) of a related porphyrin molecule. Regarding the energy gain due to the pyridyl−Cu interaction, experiments[51] as well as theory[52] agree on a binding energy of roughly 23 kcal/mol for an isolated pyridine molecule on Cu. The resulting value of 92 kcal/mol for an entire TPyP molecule thus easily compensates the energy needed for the nonplanar deformation upon adsorption.

At this point it is instructive to further discuss two issues. We already mentioned the strikingly different adsorption behavior of TPyP on Ag(111) and Cu(111). These differences can be rationalized by comparing the interactions between pyridyl molecules and the respective substrates. Indeed the bonding of pyridyl to Cu via the N lone pair proved to be very important, whereas in the case of Ag(111) the interaction with the π electrons of the aromatic ring is dominant.[53] At low coverage, this difference results in pyridyl standing upright on Cu(110) with the N pointing toward the surface,[51] whereas it prefers a rather planar adsorption geometry on Ag(111).[54]

A second comparison also corroborates the importance of the nitrogen for the reported adsorption behavior. Co−tetraphenylporphyrin (Co−TPP) is a molecule closely related to TPyP. However, it is terminated by phenyl rings and the macrocycle hosts a Co ion bonded to the four pyrrolic nitrogens. After room-temperature deposition of Co−TPP on Cu(111) we observe highly ordered compact islands of Co−TPP, evidencing that the room-temperature mobility of Co−TPP is higher than for TPyP, despite the additional interaction of the Co center with the metal substrate. Consequently, also this observation points to the decisive role the nitrogen lone pairs play for the mobility and conformation of TPyP on Cu(111).

3.3. Reactivity toward Metal Centers. A second type of bonding mechanism between the terminal pyridyl groups and metal atoms is revealed by the experiment presented in Figure 5. Single Fe atoms where added in situ at 8 K, where thermal diffusion is frozen in. Figure 5a accordingly shows randomly distributed Fe monomers appearing as round protrusions coexisting with TPyP molecules. In a next step the sample temperature was slightly increased to about 15 K, which allows the Fe adatoms to freely migrate on the surface, while the TPyP is immobile. Subsequently, the sample was cooled down again to freeze the adatom motion. As a result Fe is selectively captured by the pyridyl groups (Figure 5b). Once attached the adatoms stick and do not diffuse. The modified imaging characteristics of both Fe and TPyP endgroups indicate marked chemical interaction. Judging from the unchanged appearance of the molecular core, a relaxation of the TPyP is rather unlikely. This reveals that the conformationally adapted nonplanar pyridyl moiety qualifies for two-dimensional (2D) metallosupramolecular engineering. Interestingly, the imaging characteristics differ from the previously reported STM data of 2D mono-

(49) The saddle-shape and, in particular, the angles ρ in Figure 4, parts b and c, are obtained by optimizing the geometry of the porphyrin macrocycle by the MM+ procedure complying with the constraints given by the pyridyl conformation.

(50) Jentzen, W.; Song, X.-Z.; Shelnutt, J. A. *J. Phys. Chem. B* **1997**, *101*, 1684−1699.
(51) Lee, J.-G.; Ahner, J.; Yates, J. T., Jr. *J. Chem. Phys.* **2001**, *114*, 1414−1419.
(52) Wu, D. Y.; Hayashi, M.; Shiu, Y. J.; Liang, K. K.; Chang, C. H.; Yeh, Y. L.; Lin, S. H. *J. Phys. Chem. A* **2003**, *107*, 9658−9667.
(53) Giessel, T.; Schaff, O.; Lindsay, R.; Baumgärtel, P.; Polcik, M.; Bradshaw, A. M.; Koebbel, A.; McCabe, T.; Bridge, M.; Lloyd, D. R.; Woodruff, D. P. *J. Chem. Phys.* **1999**, *110*, 9666−9672.
(54) (a) Demuth, J. E.; Christmann, K.; Sanda, P. N. *Chem. Phys. Lett.* **1980**, *76*, 201−206. (b) Bader, M.; Haase, J.; Frank, K.-H.; Puschmann, A.; Otto, A. *Phys. Rev. Lett.* **1986**, *56*, 1921−1924.

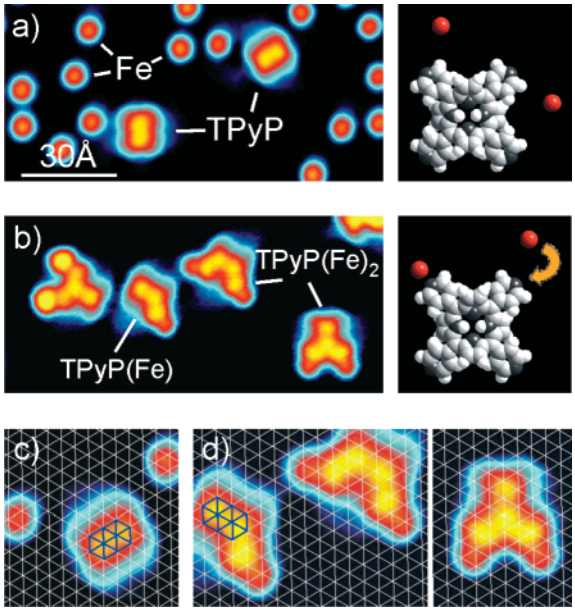

Figure 5. Selective attachment of Fe adatoms to the pyridyl groups of TPyP. (a and b: same size; panel a, $V = 30$ mV, $I = 0.2$ nA; panel b, $V = 20$ mV, $I = 0.2$ nA). See text for discussion. Two main steps of this experiment are schematically illustrated in the column on the right. (c) A detailed view of (a) which indicates that the reported TPyP adsorption site is consistent with single Fe atoms centered on hollow sites. (d) The overlaid substrate lattice grid (lattice constant 2.55 Å) exemplifies the highly symmetric appearance of the $TPyP(Fe)_n$ complexes. The blue rhombi embrace the two central protrusions (compare Figure 2).

nuclear compounds or dinuclear nanogrids, reflecting Cu− and Fe−carboxylate formation, where no effect on the ligand appearance appeared and a planar geometry of the molecular linkers is expected.[55]

In analogy to the determination of the TPyP adsorption site, we address in Figure 5, parts c and d, the Fe positions by overlaying an atomic lattice. We find that the "bridge" adsorption site of TPyP is consistent with isolated Fe adatoms occupying "hollow" sites of the underlying substrate atomic lattice (Figure 5c), an adsorption site suggested in previous reports.[56] The convolution of the molecular and atomic signatures hampers a precise and reliable determination of the positions of the Fe centers in the TPyP−Fe complexes. Nevertheless, the STM image in Figure 5d demonstrates the highly symmetric appearance and directionality of the pyridyl−Fe complex and suggests a lateral Fe−N distance of about 2.4 ± 0.5 Å. This value compares well with a Fe−pyridyl bond length of 2.2 Å reported for a three-dimensional Fe−porphyrin complex[25] and the positioning of diiron units simultaneously coordinated by carboxylate and pyridyl ligands on Cu(100).[57]

These findings confirm that the N-containing ligands retain their affinity toward metal centers despite the conformational adaptation, implying a nonplanar orientation of pyridyl groups, and directly visualize the impact of metal−ligand interactions on a metallosupramolecular self-assembly process in two dimensions where the ligands are spatially anchored. Furthermore additional incoming Fe monomers can be trapped by the metal−ligand complex, resulting in small metal clusters pinned to the pyridyl groups of the TPyP (Figure 5b, complex on the left). This approach allows one in principle to self-assemble large quantities of metal−molecule−metal bridges[58] which might prove very interesting to study metal−molecule contacts as these junctions are defined on an atomic level.[4]

4. Conclusions

The presented experiments indicate that the attractive interactions between the functional pyridyl moieties and the Cu substrate, presumably mediated by the lone pair electrons of nitrogen, not only anchor the TPyP molecules but also promote a strong deformation of the molecular geometry. Furthermore the functional pyridyl legs are strong attractors for Fe atoms. This permitted us to present snapshots of the self-assembly process of a metal−organic complex in two dimensions.

Our findings permit us to selectively attach metal centers to pyridyl moieties and open up pathways to steer the mobility of large organic molecules.

In addition, we presented a novel approach to determine the geometry of adsorbed molecules. The combination of the well-established NEXAFS method with a procedure relating calculated charge densities to high-resolution STM data presents a useful tool to study conformations of large molecular adsorbates, which should be applicable for a wide variety of systems. Therewith, we quantified for the first time the saddle-shaped geometry of an adsorbed free-base porphyrin molecule. Such structural information provides a prerequisite to control functional properties of adsorbed complex molecules and the conformational design of flexible species embedded in molecular nanoarchitectures at surfaces.

Acknowledgment. This work was supported by the Canada Foundation of Innovation (CFI), National Science and Engineering research Council of Canada (NSERC), British Columbia Knowledge Development Fund (BCKDF), and the ESF-EUROCORES-SONS Project "FunSMARTs". W.A. thanks the Swiss National Science Foundation (SNF), and A.W.-B. thanks the German Academic Exchange Service (DAAD) for financial support. Support of the travel of T.S. to the Berlin synchrotron source by the BMBF through Project No. 05 ES3XBA/5 is gratefully acknowledged.

JA071572N

(55) (a) Lin, N.; Dmitriev, A.; Weckesser, J.; Barth, J. V.; Kern, K. *Angew. Chem., Int. Ed.* **2002**, *41*, 4779−4783. (b) Messina, P.; Dmitriev, A.; Lin, N.; Spillmann, H.; Abel, M.; Barth, J. V.; Kern, K. *J. Am. Chem. Soc.* **2002**, *124*, 14000−14001. (c) Lingenfelder, M.; Spillmann, H.; Dmitriev, A.; Stepanov, S.; Lin, N.; Barth, J. V.; Kern, K. *Chem. Eur. J.* **2004**, *10*, 1913−1919. (d) Seitsonen, A. P.; Lingenfelder, M.; Spillmann, H.; Dmitriev, A.; Stepanow, S.; Lin, N.; Kern, K.; Barth, J. V. *J. Am. Chem. Soc.* **2006**, *128*, 5634−5635.

(56) Crommie, M. F.; Lutz, C. P.; Eigler, D. M. *Science* **1993**, *262*, 218−220.

(57) Lin, N.; Stepanow, S.; Vidal, F.; Barth, J. V.; Kern, K. *Chem. Commun.* **2005**, 1681−1683.

(58) Clair, S.; Pons, S.; Brune, H.; Kern, K.; Barth, J. V. *Angew. Chem., Int. Ed.* **2005**, *44*, 7294−7297.